

Evolution of electron beam pulses of short duration in the solar corona

G. A. Casillas-Pérez*

Instituto de Geofísica, Universidad Nacional Autónoma de México, Ciudad Universitaria, C.P. 04510, Ciudad de México, México.

S. Jeyakumar

Departamento de Astronomía, Universidad de Guanajuato, México, Guanajuato, Gto., C.P. 36000, México.

H. R. Pérez-Enríquez

Centro de Geociencias, Universidad Nacional Autónoma de México, Campus Juriquilla, C.P. 76230 Juriquilla, Querétaro, México.

M. A. Trinidad

Departamento de Astronomía, Universidad de Guanajuato, México, Guanajuato, Gto., C.P. 36000, México..

Abstract

Narrowband radio bursts with durations of the order of milliseconds, called spikes, are known to be associated with solar flares. In order to understand the particle beams responsible for the radio spike phenomena, evolution of electron beam pulses injected from a solar flare region into the corona is studied. Numerical integration of the Fokker-Planck (FP) equation is used to follow the evolution of the electron beam pulse. The simulations show that the short duration pulses lose most of their energy within a second of propagation into the corona. Electron beam with a small low energy cut off is thermalised faster than that with a high low energy cut off.

Keywords: Solar corona; Solar radio burst; Fokker-Planck equation;

*Corresponding author

Email address: `gacp@geofisica.unam.mx` (G. A. Casillas-Pérez)

1. Introduction

Explosive events occurring in the Sun produce radiation in a wide range of the electromagnetic spectrum. In the radio band, particularly of interest are the fast transient events known as radio spikes. These are events with enhanced radio emission with durations of the order of tens of milliseconds [Vlasov et al. (2002); Krucker et al. (1997), Bouratzis et al. (2015)], that surpass the solar radio emission of the quiet sun (Benz, 2009). The study of solar radio spikes has been of interest for some decades and has been considered to be important for understanding the physical processes occurring in the solar corona and their possible association to other large energy releasing events such as solar flares and coronal mass ejections [Chen et al. (2015), Aschwanden and Guedel (1992), Dabrowski et al. (2003), Tan et al. (2012), Tan (2013), Dabrowski et al. (2011)]. Recently, unusual radio bursts of millisecond durations were also observed to be associated with the solar flares (Oberoi et al., 2009).

There are numerous observations of solar radio spikes in different frequency bands [Guedel and Benz (1990); Fleishman et al. (2003); Vlasov et al. (2002); Magdalenic et al. (2006); Rozhansky et al. (2008); Dabrowski et al. (2011); Li (1986); Shevchuk et al. (2016)]. Observations of these spikes show positive, negative, or null drift rates over a very narrow bandwidth, which implies a small source extent for these events. These spikes have also been observed in groups from tens to thousands inside broad-band radio bursts of type I, III and IV and together with X-ray bursts. These observations indicate that the particles responsible for the radio spikes are also produced during reconnection events.

Based on the observed high brightness temperature of the radio emission, which reach values up to $10^{13} - 10^{15} K$ or higher [Benz (1986); Dabrowski et al. (2011); Vlasov et al. (2002); Aschwanden (1990)], the spikes necessarily have to be associated with a non-thermal coherent emission mechanism [Aschwanden and Guedel (1992); Benz (1986); Dabrowski et al. (2011); Vlasov et al. (2002)]. Both electron cyclotron maser (ECM) and plasma waves were proposed as candidates for the possible radio emission process. In the case of plasma waves, the magnetic field strength is not a relevant factor influencing the radio emission [Melrose (1975); Zheleznyakov and Zlotnik (1975)]. Many

observed features of radio spikes could be explained in the framework of the plasma waves [Warwick and Dulk (1969); Melnik et al. (2014)]. It is assumed that the radio emission from solar bursts is initiated by instabilities in the plasma. These instabilities cause the generation of Langmuir waves (longitudinal) which drive the generation of radio emissions by means of wave-wave interactions [Tang and Wu (2009); Li and Cairns (2013); Tan (2013); Tan (2013); Dabrowski et al. (2015)]. On the other hand, the ECM mechanism suggests that radio emission is produced by wave-particle interactions arising from loss-cone instabilities (Aschwanden, 2005). For the occurrence of the ECM emission a strong magnetic field is required, which can be expected only in dense inhomogeneities [Fleishman et al. (2003); Kuijpers et al. (1981)].

Irrespective of the emission process, fundamental to the generation of spikes is a propagating electron beam. The electrons are accelerated either during the magnetic reconnection or by propagating shocks in the solar flare region [Miller et al. (1997); Zharkova et al. (2011)]. The evolution of the electrons injected into a solar magnetic loop has been numerically studied in order to understand the phenomena of radio spikes [e.g., Aschwanden (1990)].

However, the electrons that propagate away from the acceleration site towards the outer corona produce intense radio emission with rapid drifts in frequency, known as type III radio bursts. Numerical simulations of these outward propagating electron beams were carried out in order to study the type III bursts [Ratcliffe et al. (2014); Reid and Kontar (2013); Li et al. (2008); Li et al. (2011c)]. These simulations show that the onset of Langmuir wave generation and associated onset of radio emission depends on the duration of the electron beam injection, where bursts observed at frequencies greater than about 1 GHz require beam durations of milliseconds or lower. These simulations launch the electron beam over a wide region in space estimated from type III observations. However in order to produce short duration spikes it is necessary to study the evolution of electron beam pulses of short duration injected in a smaller region, such as density inhomogeneities or micro structure on the reconnection region. Therefore in this work the evolution of short duration electron beam pulse in the solar corona, injected in a small region of space, is studied numerically. We have developed a numerical code to solve the time dependent FP equation based on the solution strategy of Hamilton et al. (1990). We use the code to study the evolution of short duration electron beam pulses. In section 2 we describe the model for the evolution of the particle distribution function. In section 3 we describe the parameters of the electron beam pulse. In section 4 the results

obtained from simulations are presented. The conclusions are presented in the section 5.

2. Model of electron beam evolution

The evolution of phase space distribution function $f(E, \mu, s, t)$ per unit volume (cm^{-3}), unit energy (KeV) and unit pitch angle cosine (μ) of electron beams propagating in the solar corona is followed at different times and position. The dominant processes that affect the energy and pitch angle of the particles are the Coulomb collisions and magnetic mirroring. In addition, such a propagating electron beam also induces an electric field and a neutralizing return current (McClements, 1992; Siversky and Zharkova, 2009).

The evolution of the energetic particle phase space distribution function can be described by the time dependent FP equation with the following terms (e.g., Lifshitz and Pitaevskii, 1981; Hamilton et al., 1990).

$$\begin{aligned} \frac{\partial f}{\partial t} + \mu c \beta \frac{\partial f}{\partial s} + \frac{\partial(\dot{\mu}f)}{\partial \mu} + \frac{\partial(\dot{E}f)}{\partial E} - \frac{e\mathcal{E}}{m_e} \mu \frac{\partial f}{\partial v} - \frac{e\mathcal{E}}{m_e v} (1 - \mu^2) \frac{\partial f}{\partial \mu} \\ = \frac{\partial}{\partial \mu} \left(D_{\mu\mu} \frac{\partial f}{\partial \mu} \right) + \left(\frac{\partial f}{\partial t} \right)_{mag-mirror} + S(E, \mu, s, t) \end{aligned} \quad (1)$$

In the above equation E is energy, μ is the cosine of the pitch angle, s is the position from the top of the coronal loop and $\beta = v/c$. The function $S(s, E, \mu, t)$ describes the source function. The variable \mathcal{E} is the electric field induced by the electron beam, e and m_e are the electron charge and mass respectively, c is the speed of light, $D_{\mu\mu}$ is the diffusion coefficient due to Coulomb collisions and v is the velocity.

Substituting the terms $\dot{\mu}$, \dot{E} and $D_{\mu\mu}$ corresponding to the magnetic mirroring and Coulomb collisions as given in Hamilton et al. (1990), the above equation can be written in scaled units as,

$$\begin{aligned} \frac{\partial f}{\partial \tau} = -\mu\beta \frac{\partial f}{\partial \xi} + \frac{\beta}{2} \frac{d \ln B}{d \xi} \frac{\partial}{\partial \mu} [(1 - \mu^2) f] + \eta \ln \Lambda \frac{\partial}{\partial E} \left(\frac{f}{\beta} \right) \\ + \frac{\eta \ln \Lambda}{\beta^2 \gamma^2} \frac{\partial}{\partial \mu} \left[(1 - \mu^2) \frac{\partial f}{\partial \mu} \right] + \alpha \varepsilon \mu \beta \frac{\partial f}{\partial E} + \alpha \frac{\varepsilon (1 - \mu^2)}{\beta} \frac{\partial f}{\partial \mu} \\ + S(E, \mu, s, t) \end{aligned} \quad (2)$$

Table 1: Parameters of the simulation runs

Run	γ	E_0 (Kev)	n_b cm ⁻³
B1	3	16	1.75×10^7
B2	3	7	1.74×10^7
B3	7	16	2.87×10^7

Here E is expressed in units of electron rest mass energy, and other scaled variables are given below.

$$\tau_c = 1/(4\pi n_0 c r_0^2) \quad \tau = t/\tau_c \quad \xi = s/(c\tau_c) \quad \eta = n/n_0 \quad \varepsilon = \mathcal{E}/\mathcal{E}_0$$

$$\alpha = \frac{e\mathcal{E}_0\tau_c}{m_e c} \quad \mathcal{E}_0 = \frac{m_e c^2}{2\pi e^3 n_0}$$

where $\ln \Lambda$ is the Coulomb logarithm which is assumed to be ≈ 10 , r_0 is the classical radius of the electron, n_0 is unit of ambient density scale and the variable n is the ambient density. The numerical schemes implemented for the energy, position and μ terms of the FP equation are based on the strategy proposed by [Hamilton et al. \(1990\)](#). The electric field \mathcal{E} can be calculated using equation 3 of [Zharkova and Gordovskyy \(2006\)](#). However, the results of the simulations reported in this work do not include the effects of the magnetic convergence nor the electric field terms, which corresponds to those with the variables ε and B on the right side of equation 2.

3. Simulation of electron beam pulse propagation

The evolution of an electron beam pulse is studied by launching a pulse of short duration from the top of a magnetic loop into the solar corona. Based on the observations of Xray emission from precipitating electron beams, the duration of the pulse is of the order of 10^{-3} s [[Charikov et al. \(2004\)](#); [Siversky and Zharkova \(2009\)](#)]. The pulse is injected at a height of 10^9 cm from the photosphere and the evolution is followed to a distance of about 3×10^{11} cm.

The electron beam is injected at the lower boundary using the boundary condition for the electron distribution function of the form,

$$f(E, \mu) = f_n \psi(\tau) \frac{(E/E_0)^{\delta-1}}{(E/E_0)^{\delta+\gamma} + 1} \exp\left(-\frac{(1-\mu)^2}{\Delta\mu^2}\right) \quad (3)$$

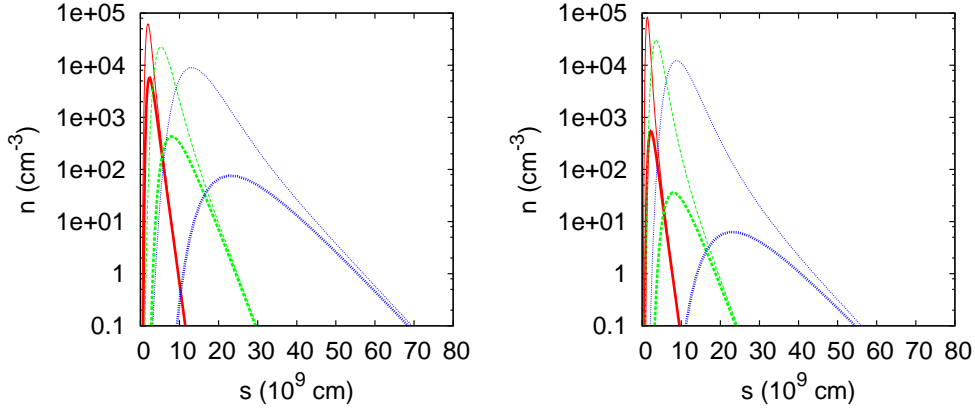


Figure 1: The total density n (cm^{-3}) as a function of position is plotted at times $t = 0.282, 0.785$ and 1.968 s as solid (red), dashed (green) and dotted (blue) curves respectively. The thin lines show results from model runs with only positional advection and the thick lines show that of the model runs including Coulomb collisions. The left and right panels correspond to model run B1 ($E_0 = 16$ KeV) and B2 ($E_0 = 7$ KeV) respectively.

where $\delta = 10$, is the power-law index of the electron distribution below the cut off energy of E_0 , and $\gamma = 3$ is the value of the power-law index for energies above E_0 , $\Delta\mu = 0.2$ is the Gaussian width of the pitch angle distribution. The range of energy of the distribution is $E_{min} = 1.2$ KeV and $E_{max} = 384$ KeV, with a cutoff energy of $E_0 = 16$ or 7 KeV. The temporal profile $\psi(\tau)$ of the beam, is taken as rectangular function with a width of 0.2×10^{-3} s. The beams are injected at the lower boundary, which corresponds to a physical size of about 100 km along the propagation direction, for the resolution used in the simulations.

The initial condition of the electron beam distribution is $f(\tau = 0, \xi, E, \mu) = 0$, and the upper boundary condition is $f(\xi_{max}, E, \mu) = f(\xi_{max} - d\xi, E, \mu)$. The ambient density profile in the corona is described (e.g. [Ratcliffe, 2013](#)),

$$n = n_0 \exp(-(s - s_0)/H_{scale}) \quad (4)$$

where $n_0 = 10^{10} \text{ cm}^{-3}$ is the density at the lower boundary and $H_{scale} = 10^{10} \text{ cm}$ is the scale height. For the range of distances where the electron beam is followed, the variation of the magnetic field is not that significant. Moreover, the effects of induced electric field on the evolution of the electron beam pulses of short duration is small ([Siversky and Zharkova, 2009](#)). Therefore as a first approximation, the simulations presented here do not include

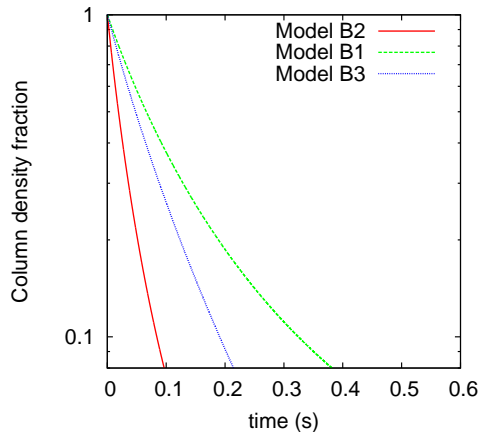


Figure 2: The ratio of column density through the simulation domain of model runs B with those of A are plotted against time. The dashed (green), solid (red) and dotted (blue) curves represent model runs B1, B2, and B3 respectively. The loss of the electron population can be seen as decreasing fraction over time.

the magnetic convergence and the electric field terms. The simulations were carried out with a resolution of 100, 30 and 30 grids in position, μ and energy axes respectively. The position and energy axes were divided logarithmically. The simulations runs were carried out for different low energy cut offs (B1 and B2) and high energy spectral index (B3). For comparison, simulations excluding all but positional affection terms were also carried out (runs A1, A2, and A3 respectively). The distribution function is normalized with a flux at the lower boundary, $F_0 = 10^{12} \text{ erg cm}^{-2} \text{ s}^{-1}$. The parameters used for the simulations and the effective total density are given in table 1

4. Results and Discussion

4.1. Effect of collisions on the propagating pulse

The variation of the density of the electrons with position is shown in the Figure 1. During the propagation of the pulse, the width widens due to the electrons with higher energies moving faster than the lower energy electrons, as can be seen more pronounced in the model runs without the effect of collisions (thin curves). In the models with collisional terms, the density decreases due to collisions of the beam particles with the ambient plasma (thick curves). For an electron spectrum with a higher low energy cut off,

the pulses widen due to the faster velocities of the electrons. The beam electrons thermalised due to collisions will ultimately leave the distribution. The total column density of electrons integrated through the simulation domain plotted in Figure 2 shows that about 90% of the beam electrons are lost due to collisions within less than a second. Although the injected electron beam pulse has a width of 160 km (0.2 millisecond after injection) along the propagation direction, the pulse width widens as it propagates. However the width of the radio emitting region depends on the conditions in the ambient medium, such as the onset of instabilities, small-scale inhomogeneities in density and magnetic field [Vlasov et al. (2002); Rozhansky et al. (2008); Li et al. (2011b); Li et al. (2011a); Li et al. (2011c); Li et al. (2012)]. In general, the temporal and spatial scales of radio emission are expected to be smaller than that seen in the simulations reported here. In order to compare the results of the simulations with the durations of the observed spikes, realistic simulations that follow the evolution of the waves are necessary.

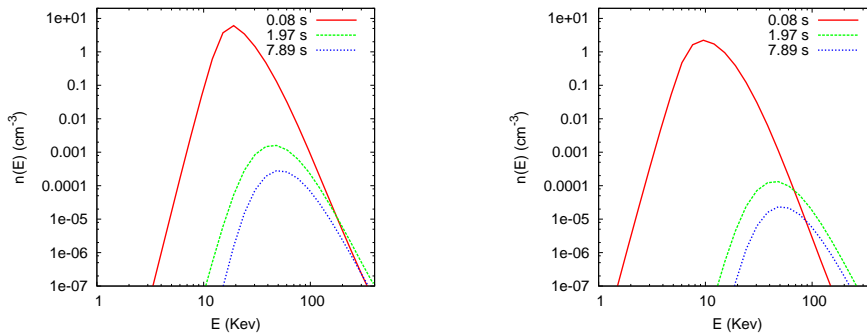


Figure 3: Spectrum at the location where the peak of the pulse occurs is plotted for the model runs B1 (left panel) and B2 (right panel). The solid (red), dashed (green) and dotted (blue) curves represent model runs at times of 0.085, 1.97 and 7.89 s respectively. At later times the peak of the spectrum shifts to higher energies due to loss of low energy electrons. Since the high energy electrons are fast moving, at a given location the high energy spectral index appears steeper than the initial injected spectral index.

4.2. Evolution of the electron spectrum

In the Figure 3, the pitch angle averaged spectrum at the peak position of the pulse are plotted for different times. The low energy electrons are removed by collisions, thus the spectrum peaks at higher energies at later times. The fast moving electrons populate the leading edge of the pulse

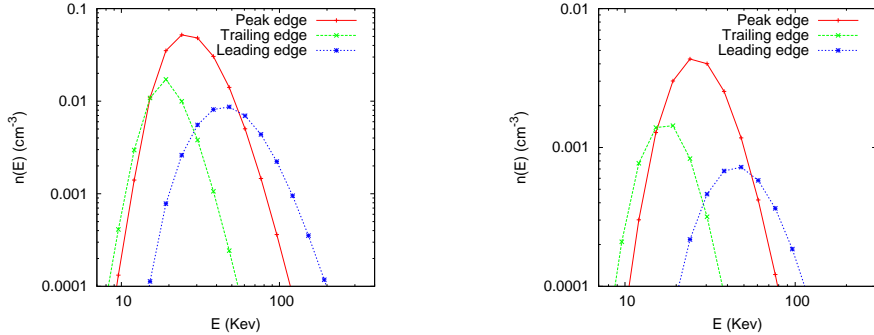


Figure 4: Spectra at the peak (solid, red), leading (dotted, blue) and trailing (dashed, green) edges of a pulse are plotted, for a time of 0.489 s. The left and right panels correspond to model run B1 and B2 respectively. The leading edge of the pulse mostly contains high energy electrons while the trailing edge contains the low energy ones.

while the trailing edge of the pulse is populated by the low energy electrons as shown in Figure 4. This can create a bump in tail distribution where $\partial f/\partial v > 0$ (Aschwanden, 2005). However, in order to estimate the radio emission, evolution of the waves generated by the electron beam has to be calculated along with the evolution of the particle distribution.

5. Conclusions

The evolution of an electron beam pulse injected from the top of the coronal magnetic loop into the corona is studied. The energetic electrons propagate faster than the low energy electrons and populate the leading edge of the pulse. Such a configuration is expected to produce radio emission by several processes induced by the beam instability. Large fraction of the electrons in a beam of short duration get thermalised within a second, as compared to the simulation of electron beams of longer duration that propagate to 1 AU. In order to produce millisecond duration with narrow bandwidth radio emission, it is necessary to simulate the propagation of short duration pulses of narrow energy bands coupled to the wave dynamics.

Acknowledgements

We thank the anonymous referees for very useful comments that have hugely improved the presentation and have helped to correct several am-

biguous statements. We also thank the referees for bringing to our notice earlier papers on numerical simulations related to this work. Gilberto A. Casillas-Pérez thanks IGF-UNAM and DGAPA-UNAM for the support and grant offered during the research project. This work was partially supported by PROMEP/103-5/07/2462 and Conacyt CB-2009-01/130523 grants.

References

- Aschwanden, M. J., Nov. 1990. Relaxation of the loss-cone by quasi-linear diffusion of the electron-cyclotron maser instability in the solar corona. *A&AS* 85, 1141–1177.
- Aschwanden, M. J., 2005. *Physics of the Solar Corona. An Introduction with Problems and Solutions*. 2nd. edn. Springer-Verlag, Berlin.
- Aschwanden, M. J., Guedel, M., Dec. 1992. The coevolution of decimetric millisecond spikes and hard X-ray emission during solar flares. *ApJ* 401, 736–753.
- Benz, A. O., Mar. 1986. Millisecond radio spikes. *Sol. Phys.* 104, 99–110.
- Benz, A. O., 2009. *Solar System*. Springer-Verlag, Berlin.
- Bouratzis, C., Hillaris, A., Alissandrakis, C. E., Preka-Papadema, P., Mousas, X., Caroubalos, C., Tsitsipis, P., Kontogeorgos, A., Jan. 2015. Fine Structure of Metric Type IV Radio Bursts Observed with the ARTEMIS-IV Radio-Spectrograph: Association with Flares and Coronal Mass Ejections. *Sol. Phys.* 290, 219–286.
- Charikov, Y. E., Dmitriyev, P. B., Koudriavtsev, I. V., Lazutkov, V. P., Matveev, G. A., Savchenko, M. I., Skorodumov, D. V., 2004. Solar flare hard X-rays measured by spectrometer "IRIS": spectral and temporal characteristics. In: Stepanov, A. V., Benevolenskaya, E. E., Kosovichev, A. G. (Eds.), *Multi-Wavelength Investigations of Solar Activity*. Vol. 223 of IAU Symposium. pp. 429–432.
- Chen, B., Bastian, T. S., Shen, C., Gary, D. E., Krucker, S., Glesener, L., Dec. 2015. Particle acceleration by a solar flare termination shock. *Science* 350, 1238–1242.

- Dabrowski, B., Rompolt, B., Falewicz, R., Rudawy, P., Siarkowski, M., Sep. 2003. Relationship between solar radio spikes observed at 1420 MHz and solar active phenomena. In: Wilson, A. (Ed.), *Solar Variability as an Input to the Earth's Environment*. Vol. 535 of ESA Special Publication. pp. 491–494.
- Dabrowski, B. P., Karlický, M., Rudawy, P., Jan. 2015. Fourier Analysis of Radio Bursts Observed with Very High Time Resolution. *Sol. Phys.*290, 169–180.
- Dąbrowski, B. P., Rudawy, P., Karlický, M., Nov. 2011. Millisecond Radio Spikes in the Decimetric Band. *Sol. Phys.*273, 377–392.
- Fleishman, G. D., Gary, D. E., Nita, G. M., Aug. 2003. Decimetric Spike Bursts versus Microwave Continuum. *ApJ*593, 571–580.
- Guedel, M., Benz, A. O., May 1990. Time profiles of solar radio spikes. *A&A*231, 202–212.
- Hamilton, R. J., Lu, E. T., Petrosian, V., May 1990. Numerical solution of the time-dependent kinetic equation for electrons in magnetized plasma. *ApJ*354, 726–734.
- Krucker, S., Benz, A. O., Aschwanden, M. J., Jan. 1997. YOHKOH observation of the source regions of solar narrowband, millisecond spike events. *A&A*317, 569–579.
- Kuijpers, J., van der Post, P., Slottje, C., Nov. 1981. Runaway acceleration in a radio flare. *A&A*103, 331–338.
- Li, B., Cairns, I. H., Feb. 2013. Type III Radio Bursts in Coronal Plasmas with Kappa Particle Distributions. *ApJ*763, L34.
- Li, B., Cairns, I. H., Robinson, P. A., Jun. 2008. Simulations of coronal type III solar radio bursts: 1. Simulation model. *Journal of Geophysical Research (Space Physics)* 113, A06104.
- Li, B., Cairns, I. H., Robinson, P. A., Mar. 2011a. Effects of Spatial Variations in Coronal Electron and Ion Temperatures on Type III Bursts. II. Variations in Ion Temperature. *ApJ*730, 21.

- Li, B., Cairns, I. H., Robinson, P. A., Mar. 2011b. Effects of Spatial Variations in Coronal Temperatures on Type III Bursts. I. Variations in Electron Temperature. *ApJ*730, 20.
- Li, B., Cairns, I. H., Robinson, P. A., Jul. 2012. Frequency Fine Structures of Type III Bursts Due to Localized Medium-Scale Density Structures Along Paths of Type III Beams. *Sol. Phys.*279, 173–196.
- Li, B., Cairns, I. H., Yan, Y. H., Robinson, P. A., Sep. 2011c. Decimetric Type III Bursts: Generation and Propagation. *ApJ*738, L9.
- Li, H. W., Mar. 1986. Hollow beam distribution of energetic electrons and higher harmonics of electron cyclotron maser. *Sol. Phys.*104, 131–136.
- Lifshitz, E. H., Pitaevskii, L. P., 1981. *Physical Kinetics*. Pergamon Press, Oxford.
- Magdalenić, J., Vršnak, B., Zlobec, P., Hillaris, A., Messerotti, M., May 2006. Classification and Properties of Supershort Solar Radio Bursts. *ApJ*642, L77–L80.
- McClements, K. G., May 1992. The simultaneous effects of collisions, reverse currents and magnetic trapping on the temporal evolution of energetic electrons in a flaring coronal loop. *A&A*258, 542–548.
- Melnik, V. N., Shevchuk, N. V., Konovalenko, A. A., Rucker, H. O., Dorovskyy, V. V., Poedts, S., Lecacheux, A., May 2014. Solar Decameter Spikes. *Sol. Phys.*289, 1701–1714.
- Melrose, D. B., Jul. 1975. Small-scale inhomogeneities in the solar corona - Evidence from meter-wavelength radio bursts. *Sol. Phys.*43, 79–86.
- Miller, J. A., Cargill, P. J., Emslie, A. G., Holman, G. D., Dennis, B. R., LaRosa, T. N., Winglee, R. M., Benka, S. G., Tsuneta, S., Jul. 1997. Critical issues for understanding particle acceleration in impulsive solar flares. *J. Geophys. Res.*102, 14631–14660.
- Oberoi, D., Evarts, E. R., Rogers, A. E. E., Dec. 2009. High Temporal and Spectral Resolution Interferometric Observations of Unusual Solar Radio Bursts. *Sol. Phys.*260, 389–400.

- Ratcliffe, H., 2013. Electron beam evolution and radio emission in the inhomogeneous solar corona. Ph.D. thesis, University of Glasgow (United Kingdom).
- Ratcliffe, H., Kontar, E. P., Reid, H. A. S., Dec. 2014. Large-scale simulations of solar type III radio bursts: flux density, drift rate, duration, and bandwidth. *A&A*572, A111.
- Reid, H. A. S., Kontar, E. P., Jul. 2013. Evolution of the Solar Flare Energetic Electrons in the Inhomogeneous Inner Heliosphere. *Sol. Phys.*285, 217–232.
- Rozhansky, I. V., Fleishman, G. D., Huang, G.-L., Jul. 2008. Millisecond Microwave Spikes: Statistical Study and Application for Plasma Diagnostics. *ApJ*681, 1688–1697.
- Shevchuk, N. V., Melnik, V. N., Poedts, S., Dorovskyy, V. V., Magdalenic, J., Konovalenko, A. A., Brazhenko, A. I., Briand, C., Frantsuzenko, A. V., Rucker, H. O., Zarka, P., Jan. 2016. The Storm of Decameter Spikes During the Event of 14 June 2012. *Sol. Phys.*291, 211–228.
- Siversky, T. V., Zharkova, V. V., Sep. 2009. Stationary and impulsive injection of electron beams in converging magnetic field. *A&A*504, 1057–1070.
- Tan, B., Aug. 2013. Small-scale Microwave Bursts in Long-duration Solar Flares. *ApJ*773, 165.
- Tan, B., Yan, Y., Tan, C., Sych, R., Gao, G., Jan. 2012. Microwave Zebra Pattern Structures in the X2.2 Solar Flare on 2011 February 15. *ApJ*744, 166.
- Tang, J. F., Wu, D. J., Jan. 2009. Electron-cyclotron maser emission by power-law electrons in coronal loops. *A&A*493, 623–628.
- Vlasov, V. G., Kuznetsov, A. A., Altyntsev, A. T., Feb. 2002. The maser mechanism for solar millisecond spike generation in inhomogeneous plasma. *A&A*382, 1061–1069.
- Warwick, J. W., Dulk, G. A., Nov. 1969. Spectrum and Polarization of Solar Radio Bursts on a 10-MILLISECOND Time Scale. *ApJ*158, L123–L125.

- Zharkova, V. V., Arzner, K., Benz, A. O., Browning, P., Dauphin, C., Emslie, A. G., Fletcher, L., Kontar, E. P., Mann, G., Onofri, M., Petrosian, V., Turkmani, R., Vilmer, N., Vlahos, L., Sep. 2011. Recent Advances in Understanding Particle Acceleration Processes in Solar Flares. *Space Sci. Rev.*159, 357–420.
- Zharkova, V. V., Gordovskyy, M., Nov. 2006. The Effect of the Electric Field Induced by Precipitating Electron Beams on Hard X-Ray Photon and Mean Electron Spectra. *ApJ*651, 553–565.
- Zheleznyakov, V. V., Zlotnik, E. Y., Oct. 1975. Cyclotron wave instability in the corona and origin of solar radio emission with fine structure. III. Origin of zebra-pattern. *Sol. Phys.*44, 461–470.